applied sciences

MDPI

Article

An Efficient Spring Model for an Integrated Orthodontic Tooth Movement: A Verified Mathematical Model

Shai Yona [1], Oded Medina [2,†], Rachel Sarig [3,4,†] and Nir Shvalb [2,*,†]

1 The Department of Industrial Engineering, Faculty of Engineering, Ariel University, Ariel 4070000, Israel
2 The Department of Mechanical Engineering, Faculty of Engineering, Ariel University, Ariel 4070000, Israel
3 The Department of Oral Biology, The Department of Orthodontics, Maurice and Gabriela Goldschleger, School of Dental Medicine, Sackler Faculty of Medicine, Tel Aviv University, Tel Aviv 6997801, Israel
4 Dan David Center for Human Evolution and Biohistory Research, Sackler Faculty of Medicine, Tel-Aviv University, Tel Aviv 6997801, Israel
* Correspondence: nirsh@ariel.ac.il
† These authors contributed equally to this work.

Abstract: Orthodontic tooth movement is of interest to both the medical and the engineering communities. Recent studies focused their attention mainly on the stress distribution within the periodontal ligament and the surrounding alveolar bone prior to the remodeling stage. Yet, although motion is indeed triggered by the exerted stress distribution, these remodeling processes are the main driver for significant (and permanent) tooth movements. Other studies attempted to provide such a holistic mechanical model for both the stress distribution and the remodeling processes to describe the movement of the tooth along an orthodontic treatment. Nevertheless, these methods are cumbersome and slow to run, and therefore, are unlikely to provide a clinical decision support platform. This paper aims to bridge this gap by providing a relaxed, simplified numerical model. The scheme is described, and its limitations and main assumptions are stated. The model is then optimized to accommodate clinical accuracy needs. Lastly, validation is provided by comparing the model to a recent study, which demonstrates the good agreement between the model and actual real-world clinical cases.

Keywords: dentistry; tooth movement; periodontal ligament (PDL); tooth; orthodontic; remodeling

Citation: Yona, S.; Medina, O.; Sarig, R.; Shvalb, N. An Efficient Spring Model for an Integrated Orthodontic Tooth Movement: A Verified Mathematical Model. *Appl. Sci.* **2023**, *13*, 5013. https://doi.org/10.3390/app13085013

Academic Editors: Dorina Lauritano and Andrea Scribante

Received: 15 February 2023
Revised: 13 April 2023
Accepted: 15 April 2023
Published: 17 April 2023

1. Introduction

Orthodontic tooth movement (OTM) is initiated and controlled by mechanical stimuli generated by forces applied on the crown of the tooth [1]. The forces are partially governed by the periodontal ligament (PDL), which connects the teeth to the surrounding alveolar bone and decreases the rigidity of the jaw [2]; thus, the stress–strain responses of teeth and the PDL to orthodontic loading are of importance (i.e., for better understanding and for improving orthodontic yield). OTM is governed by several factors, some of which are not completely known for each patient, such as the PDL properties (i.e., thickness, stiffness, etc.) [3]. The applied forces, if not sufficiently known [4], might result in clinical side effects, such as uncontrolled tipping of the tooth or excessive stresses on the root apex that may result in root resorption. Therefore, revealing the stress–strain responses of the teeth, alveolar bone and PDL to orthodontic loading is of great importance in order to apply optimal forces during treatment. It may also be beneficial for studies of new orthodontic techniques, such as clear aligners [5]. Moreover, recent studies, such as [6], which suggest the use of machine learning in orthodontics may benefit from an efficient OTM model, such as the one suggested here.

The PDL width ranges from 0.15 to 0.38 mm and consists of 53–74% collagen fibers (see [2,7]). The literature specifies a wide range of the PDL modulus of elasticity—some suggest a range of 6–12 MPa [8]; however, most specify values of 0.6–1.2 Mpa [2,9–15].

Moreover, it is worth mentioning that the modulus of elasticity is reported to be dependent on the strain rate [16]. The PDL, as a soft tissue, has viscoelastic, inhomogeneous, anisotropic and nonlinear properties [17], but is commonly approximated to have isotropic behavior [9,12,18,19], and so we shall assume thus here.

The alveolar bone's inner structure consists of an interconnected network of trabecular rods and plates, while its outer shell presents with the more compact structure of a cortical bone [7].

The biological process of orthodontic tooth movement includes three stages [20]. (1) The first is tooth movement within the dental alveolus, with no substantial deformation upon the bone. (2) The second is a biological process, during which no movement takes place. This stage is triggered when force is applied to the tooth and is completed after a sufficient time period. (3) Once the second stage is completed, the last stage of the alveolar bone remodeling begins, during which the bone is resorbed and formed, depending on the nature of the stresses exerted upon it (i.e., compression or tension). The main portion of tooth movement occurs during this stage.

In what follows, the biological stages are modeled first as an instantaneous tooth elastic transformation, which aims to reduce the system's total energy. This is followed by an irreversible bone remodeling, which aims to reduce the (local) energy of each individual PDL fiber (see Figure 1). Yet, note that at the end of this process, the total energy of the system as a whole will not assume a minimum value.

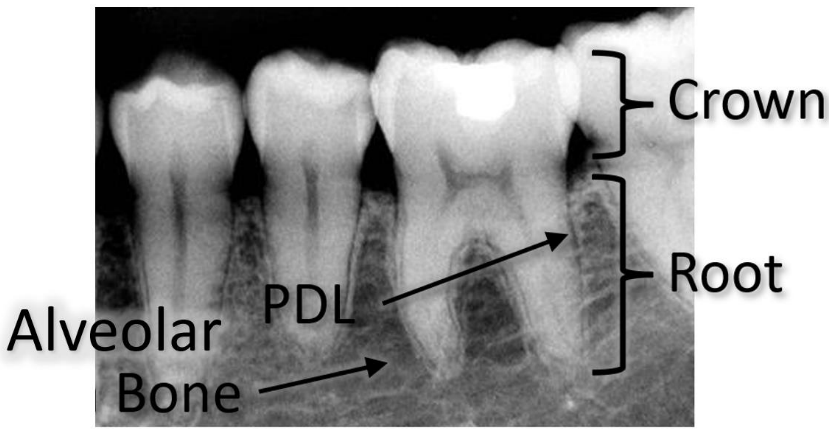

Figure 1. Tooth relevant components under X-ray imaging.

Sparse research results provide force magnitudes that were tested and produced good treatment results [21]. For example, Lee [22] recommended the usage of an optimum force of 150–260 gf with a range of applied stress of 165–185 gf/cm^2 or a bit higher, and later on, the same author [23] suggested an average stress of 197 gf/cm^2 where a minimal 1500 μ strain is required for the remodeling process to take place [17,24]. However, measuring the pressure and strain in vivo in the microenvironments of the tissues involved in tooth movements is still not applicable [3,7].

Due to the lack of rigor, orthodontists commonly classify the applied forces as light forces or heavy forces (below or above 100 gf, respectively), which, from experience, are known to produce different apparent results (e.g., sustained heavy force may result in an increase in bone mass and/or structural rearrangement, while light forces will not [25]).

The bone resorption and formation processes are quite involved (e.g., the instants in which these processes initiate are not fully known). Schepdeal et al. [13] noted that the bone resorption process is faster than bone formation. For example, 2–3 weeks of resorption may require 3 months of bone formation for replacement; however, since the orthodontic movement is directed towards the resorption side, the movement rate is limited by the bone resorption rate. The mechanics of tooth movement due to these forces is of interest to the research and orthodontist communities, most of which rely on finite element methods

(FEMs) for simulation purposes (cf. [3,11,12,19,26]). A somewhat different approach is provided in [27], in which the authors suggest a simulation of the gingival surface mesh instantaneous deformation in orthodontics by the Mass–Spring mesh model, where the PDL tissue is represented by a triangular mesh of masses linked to its neighbors by springs and dumpers, yielding a set of equations that may be numerically solved. Dot et al. [28] offered a numerical model based on the FEM method derived from CBCT scans coupled with intraoral scanner images.

Limbert et al. [29] developed constitutive laws for modeling PDLs using FEM based on continuum fiber-reinforced composites theory and defined a transversely isotropic nonlinear strain energy function. Yet, note that these studies focus their attention on the intermediate stress distributions rather than the actual tooth movement, while a holistic model of tooth movement should address the remodeling process, as well.

Initial attempts to address the entire OTM process was first made by Bourauel et al. in 1999 [30]. In their paper [30], the researchers tested the now well-established assumption that deformations of the PDL are the key stimulus for orthodontic tooth movement (a similar work was provided in [31]). Later on, Lee et al. [32] introduced a method that monitors every stage of treatment by means of optical impressions to correlate their FEM analysis with the clinically observed movements (cf. [33,34]). In 2021 Luchian et al. assessed the effect of orthodontic load over the periodontium using the FEM approach [35]. To simulate the remodeling process in each given instant, one is required to re-mesh the alveolar bone model whenever reaching an intermediate equilibrium [3]. This approach is a time-consuming procedure, on top of requiring an enormous number of model nodes. In a more recent study [3], Hasegawa et al. aimed to overcome the time-consuming procedures by applying an image-based voxel level set method on the infinitesimally translated tooth (after remodeling) and used it as their new mesh model for their iterative procedure.

Here, a fast scheme is proposed for retrieving orthodontic tooth movement, using a simplified spring model to calculate the intermediate stress distribution and the corresponding tooth movement (translation and rotation). The remodeling process, during which the developed stresses are relaxed, is also taken into consideration. This two-step process is repeated until equilibrium is reached. By employing this approach, a computer-aided design of long-term clinical treatments and their expected stress distributions at each step can be facilitated. Furthermore, relevant research studies that attempted to provide a numerical model for OTM are rarely validated against clinical data [28]; therefore, a brief clinical validation will be provided in this study.

2. The Orthodontic Mathematical Model

Based on the behavior and the biological processes of the relevant tissues described in Section 1, a numerical model to calculate the movement and stresses of the treated tooth is formulated. In the proposed model, the PDL is considered isotropic [19]; in addition, the spatial shape of the tooth is assumed to be known (e.g., by a CBCT scan). The PDL properties (thickness and modulus of elasticity) can be estimated according to literature data (Tables 1–3). Currently, the PDL thickness and shape can be determined directly by applying the Hounsfield scale [36] according to a CT scan. However, it is expected that in the future, CBCT scans, which are much more common, will improve, and their resolution will suffice and enable one to extract the PDL thickness [37,38].

Table 1. Acceptable PDL thickness in literature.

Citation	PDL Thickness [mm]
[39]	0.125–0.375
[7,10]	0.15–0.38
[9]	0.229
[40]	0.15–0.25
[3]	0.225, 0.5

Table 2. Acceptable PDL range of strains or stresses in OTM. The maximal strains or stresses in the remodeling stage are denoted by ε_M or σ_M. Beyond these values, significant pathological biological processes may occur. These may require adjustments in the model, which is beyond the scope of this research. The minimal strain ε_m required for the remodeling process to take place is considered in the proposed model.

Citation	ε_M or σ_M	ε_m
[17]	$3000\mu_{strain}$	$1000–1500\mu_{strain}$
[7]	$3000\mu_{strain}$	$1500\mu_{strain}$
[41]	-	$1500\mu_{strain}$
[12]	16 [KPa]	-

Table 3. Acceptable PDL elasticity modulus and Poisson ratio values.

Citation	PDL Young Modulus [MPa]	PDL Poisson Ratio
[2,9–11,13–15]	0.66–0.69	0.45–0.49
[12]	1.18	0.45
[39]	44	0.49
[42]	-	0.45
[8]	0.5	-
[35]	0.71	0.4
[3]	0.17	0.4
[43]	0.1–0.3 (shear modulus)	-

2.1. Instantaneous Behavior of the PDL

The extracted tooth geometry is provided as a set of faces $\mathcal{F}$ (commonly in STL file format). The PDL is modeled as a set of springs, each of which is connected to the center of a tooth face, while its other end is anchored to the surface of the alveolar bone. The system energy relaxes by changing the tooth position and orientation towards equilibrium under the orthodontic force and PDL stress. Therefore, to calculate the PDL springs' elastic energy, one should be provided with the tooth shape. Each spring $i \in I$, positioned on the i^{th} face $F_i \in \mathcal{F}$, is given two mechanical coefficients: a linear stiffness coefficient k_{ℓ_i} and a shear stiffness k_{S_i}; both are normalized to the relative area A_i they occupy. The latter is introduced to define the relaxed spring configuration as normal to its associated face. Following the conclusions of [9], one sets the i^{th} spring to be normal to the i^{th} face area. Recalling that the PDL is assumed to be isotropic tissue having a Poisson ratio of $\nu = 0.45$ (Table 3), the isotropic assumption also implies the connection $G = \mathrm{E}/(2+2\nu)$ [44], from which one can extract a connection between the k_{S_i} and k_{ℓ_i} values.

Moreover, as the PDL tissue is thin ($\sim$ 0.3 mm), a single layer of springs will suffice to model it, as depicted in Figure 2. As expected, the shear strain in all our simulation studies did not exceed 4°, so the small-angle assumption holds. The orthodontic appliances are also modeled as springs (as in most cases, they are indeed springs).

To account for the six-dimensional tooth movements (three-dimensional translations and three-dimensional rotations), all calculations were conducted in the configuration space. To do so, define the elastic energy of a tooth configuration $c \in \mathcal{C}$ as the sum of all (PDL) springs' energies and those of the external orthodontic springs:

$$U^{tot} = \sum U_i^{PDL} + \sum U_j^{ext} \tag{1}$$

where the energy of the i^{th} PDL spring is given by:

$$U_i^{PDL} = \frac{k_{\ell_i} \Delta \ell_i^2}{2} + \int_0^{\theta_i} M_i d\theta \tag{2}$$

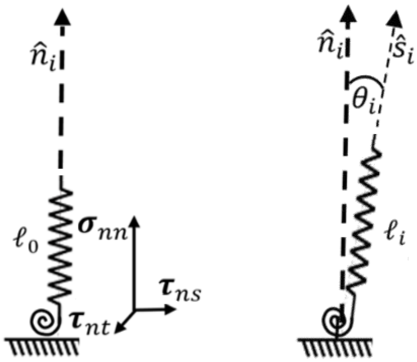

Figure 2. PDL model: A single spring block occupying a portion of the tooth surface (lower end) is anchored to the alveolar bone (upper end). Each block is comprised of paired linear and torsional springs (**left**). The springs undergo both linear $\ell_i - \ell_0$ and shear $\tan(\theta_i)$ deformations (**right**), where ℓ_0 denotes the spring's initial length.

The tensile stiffness coefficient k_{ℓ_i} is $A_i E / l_0$. In the second term, the integrand M is the torque given by $M = Fl\cos\theta$. Since $F_i = \tau_i A_i$ and $\tau_i = Gtan\theta_i$, where G is the shear modulus of the PDL, this implies that $M_i = GA_i l_i \sin\theta_i$. The change in length of the linear spring is marked by $\Delta\ell_\text{i} = \ell - \ell_0$, and θ_i denotes the angle between the spring and the tooth face normal (see Figure 2). Obviously, the total energy U^{tot} should be relaxed with each incremental step so that it approaches a minimum value at equilibrium.

As indicated, the tooth configuration c is defined as the 6-vector:

$$\mathcal{C} \ni c = (x, y, z | \theta x, \theta y, \theta z)$$

Describing the tooth's centroid position, followed by its orientation, $\mathcal{C}$ indicates the six-dimensional configuration space—the totality of the allowed tooth positions and orientations. Apply the gradient descent method [45] to advance at each timestep m towards the intermediate solution. In other words, one follows the gradient:

$$\nabla U^{tot} = \left(\frac{\partial}{\partial x}, \frac{\partial}{\partial y}, \frac{\partial}{\partial z}, \frac{\partial}{\partial \theta_x}, \frac{\partial}{\partial \theta_y}, \frac{\partial}{\partial \theta_z} \right) U^{tot}$$

and applies:

$$c_{m+1} = c_m - \varepsilon \nabla U^{tot} \tag{3}$$

at each timestep. Here, ε is a predetermined coefficient that ensures an efficient algorithm convergence. Note that Equation (1) only has a single minimum with respect to $\Delta\ell_i$ and $tan\theta_i$ for all $i \in I$ since θ_i has a limited range. This is so because the PDL fibers are bound to the free space above the tooth surface.

Figure 3 illustrates such a movement due to an orthodontic force where remodeling behavior was disabled. Note that for display purposes, the PDL is set tissue with excessive thickness located only on the top apex of the tooth, and the orthodontic force is exaggerated.

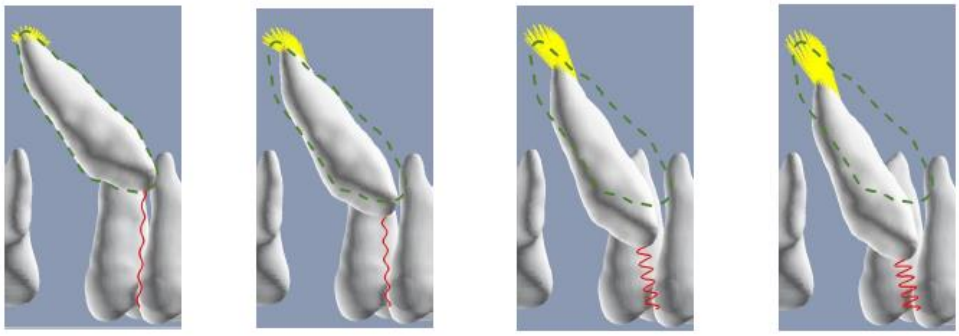

Figure 3. Spring model for instantaneous tooth movement under an external force (red). For display purposes, the PDL length is exaggerated, and only a fraction of the ligament is shown (yellow). The start position of the tooth is overlayed (green).

During the energy reduction process, springs that exceeded the edge of the alveolar bone due to tooth movement were removed. This corresponds to a situation where PDL fibers are severely damaged.

Lastly, it should be noted that throughout this paper, it is assumed that the boundary of the alveolar bone is a plane (depicted in Figure 10 as a mesh). Although it is believed that this is sufficient, future work will examine the importance of applying a curved surface based on the exact shape of the gums, which may result in more accurate outcomes.

PDL Compression Constraints

A physically sound model for OTM may be that while the PDL is overloaded, it undergoes a strain-hardening process as the alveolar bone alters its elasticity, and as a result, bone remodeling takes place [3]. Here, a simplified approach is considered, where each spring is limited to its elastic linear behavior, with a maximal allowed strain limit. It should be noted, though, that this is merely a simplified model since tissue damage processes in the biological PDL are likely to occur in cases, which exceeds this limit. Nevertheless, the simulation bone remodeling relaxes the PDL; hence, this limit hardly takes place throughout the OTM simulation, and when it does, it is only local.

Recall that the PDL tissue can be compressed up to a given limit, beyond which the resistance of the tissue becomes large enough to prevent further elastic movement. This is modeled by applying a minimal length constraint of the spring's projection on the normal n_i of the tooth face F_i. Marking the associated spring vector by s_i, this may be formalized as the inequality:

$$\hat{n}_i \cdot \hat{s}_i \geq r_i \tag{4}$$

where ℓ_i is the spring's relaxed length, and r_i is the minimal ratio for each $i \in I$. A fixed value $r_i = 0.4$ was set for all $i \in I$ to prevent the PDL tissue thickness from dropping below 40% of the original thickness (see Figure 2). To account for the set of constraints for all $i \in I$ upon violation, the six-dimensional movement of the tooth should agree with the constraint (negative) gradients.

Specifically, if a spring $i \in I$ is over-compressed, the corresponding constraint is added to the lists of the "currently active" constraints. The final trajectory is determined as the product of the tooth movement trajectory, which reduces the overall energy (Equation (1)), and the null space to the list of constraints. The result is a tooth movement, which corresponds to a path in $\mathcal{C}$ that "crawls" over the set of currently active constraints [46].

The set of constraints may be formalized as a matrix $C_{r\times 6}$, with r the number of over-compressed springs. Since each constraint reduces the dimension of the preliminary movement trajectory by 1, the remaining trajectory dimension is $6 - dim(C_{r\times 6})$. Therefore, whenever six springs or more are over-compressed, no movement is allowed.

In this situation, the remodeling step should be applied. This reflects a biological stage where tissue cannot be further compressed, and the bone resorption stage is triggered. This almost completes the model for the instantaneous spatial movement of the tooth. Next, we introduce the shear stiffness to account for the remodeling process.

Since the remodeling process relaxes the PDL springs, the highest mean stress values averaged over the tooth surface are typically introduced just before the remodeling process starts. However, the maximum stress over the tooth surface often appears after the remodeling process begins.

2.2. Remodeling Process

The remodeling process is modeled as the anchorage displacement of the springs. For example, the i^{th} pair of springs depicted in Figure 2, which is subjected to a strain, will eventually result in a movement of the anchorage point when the remodeling process initiates. The rate at which the repositioning of the i^{th}-associated springs takes place depends on the exerted strains $\varepsilon_i = \frac{\Delta\ell_i}{L}$ and $\varepsilon_{si} = tan(\theta_i)$, yielding the stresses $\sigma_i = E\epsilon = \frac{k_{\ell_i}\Delta\ell_i}{A_i}$ and $\tau_i = Gtan(\theta_i) = \frac{k_{S_i}tan(\theta_i)}{\ell_i A_i}$. Note that our model also applies when the tooth undergoes pure rotation. For clarity, recall that the remodeling stage initiates when no instantaneous movement can be applied. Resorption refers to the case where the PDL springs' length changes towards their neutral length, removing bone tissue, while formation refers to the case where the PDL springs shorten. Moreover, the remodeling process is not uniformly distributed. In every instant, some PDL springs may undergo remodeling, while others will not. Explicitly, remodeling occurs under the following stress criterion, which is directly derived from the strains criterion:

$$\sigma_m < \sigma_i < \sigma_M \tag{5}$$

For values above σ_M, the behavior of the PDL significantly differs, and thus, it is beyond the scope of this study. σ_m is the corresponding stress that realizes the minimal $1500\mu_{strain}$ requirement (Table 1). Equation (6) describes the repositioning Δs_i of the spring anchorage in the alveolar bone due to the tensile stress.

$$\Delta s_i = \Delta\ell_i k_{\ell_i}\beta_\ell \hat{s}_i + tan(\theta_i)\beta_s \frac{G(\ell_0\hat{n}_i - \ell_i\hat{s}_i)}{\ell_i \parallel \ell_0\hat{n}_i - \ell_i\hat{s}_i \parallel} \tag{6}$$

This encapsulates the fact that the spring anchoring point s_i aims to align back (Figure 2). k_{ℓ_i} and k_{S_i} are the normal and shear coefficients of spring i, and θ_i is the angle between the spring and the normal to i-th facet. The force-to-distance conversion coefficient is denoted β_ℓ and is set to 1 for formation and to 4 for resorption, reflecting the acceptable resorption and formation rates' ratio. β_s is 1 since tangent movement is symmetric in all directions in the isotropic assumption. Equation (6) implies that the anchorage movement rate is proportional to the stress applied upon the spring.

Apart from straining the PDL fibers in their longitudinal axes, the PDL has incompressible qualities that should be accounted for in the model. The magnitude of the tangent stress is calculated using the properties of the shear modulus for isotropic materials:

$$\frac{E}{2(1+\nu)} = G = \frac{F_s}{A}cot(\theta_i) \tag{7}$$

Here, E, G and ν are the PDL modulus, shear modulus and Poisson ratio, respectively, and recall Hooke's law for shear stress $\tau = G\tan\theta$. Therefore, the new position of the spring's anchorage is the accumulation of the movements due to strains in the PDL fibers' directions and shear strains.

2.3. The Combined Orthodontic Process

As mentioned, orthodontic tooth movement is modeled as a sequence of instantaneous tooth transformations and bone remodeling. However, tooth movement is an instant occurrence, while remodeling is a formation and resorption processes of the tissue requiring longer periods of time. With that said, for each iteration, one should first verify that the equivalent forces applied by the orthodontic appliance and the PDL springs exceed a minimal value that will result in non-negligible tooth movement (Table 2). Otherwise, if the PDL springs' compression/tension strains are above the predefined threshold, remodeling initiates (i.e., remodeling occurs once tooth movement reaches equilibrium). The remodeling process continues reducing the PDL total energy, while increasing the overall energy, since the applied appliance and PDL equivalent forces are in different directions. The process continues until the net generalized force vanishes, and the procedure ends (see Algorithm 1). By trial and error the translation threshold is determined to be 10^{-4} times the PDL thickness, where the angular threshold is $tan^{-1}\left(\frac{tooth\ mean\ radius}{translation\ threshold}\right)$. The pseudo code is provided below.

Algorithm 1: Tooth orthodontic movement pseudo-code

```
While Appliance connected do
    If Orthodontic force—PDL springs not in equilibrium (threshold) then
        Apply tooth movement
    else if PDL springs not in equilibrium(threshold)
        Apply remodeling
    else
        break loop
    end if
    if reached required movement then
        Disconnect appliance (loop ends)
    end if
end while
```

The stress distribution over the tooth, and, more specifically, on its root, is a valuable piece of information for clinicians. This is so since, for example, when stresses exceed a certain value, an undesirable side effect called the root resorption process may be triggered. Following the above, the normal stress and shear stress are calculated at each time stamp $\{(\sigma_{nn}, \tau_{ns}, \tau_{nt})\}_{i \in I}$; therefore, the "equivalent" von Mises stress [47] can be extracted:

$$\sigma_{i,max} = \sqrt{\sigma_{nn}^2 + 3\left(\tau_{ns}^2 + \tau_{nt}^2\right)}$$

It should be noted, though, that the rationale behind von Mises stress is based on the premise that the material fails by shear strain, which, to the authors' knowledge, is a claim that has not yet been examined. Figure 10 depicts the von Mises stress distribution when subjected to an orthodontic force compared to the applied torque. The von Mises stress values presented are low due to the remodeling process.

3. Results

FEM models for OTM typically consist of > 1 M degrees of freedom (for example, [3]). Here, since our entire model was specially designed for OTM analysis, we can make do with much less. Specifically, since the actual PDL is comprised of short fibers, it suffices to introduce only two springs normal to each tooth facet, as depicted in Figure 2, to model its behavior. However, to accommodate clinical accuracy needs, a series of tests was conducted. For this purpose, an upper canine was subjected to a 300 gf (2.94 N) load with 26,608 facets, 6652 facets, 1662 facets and 830 facets calculated in the initial loading stage before the remodeling process commences (see Figure 4). The model was then tested under the same conditions where remodeling takes place until a 0.5 mm movement of the coil anchorage point was obtained (Figure 6). Our results show that, qualitatively, these choices exhibit very similar behavior. To quantify the differences, 32 experiments were conducted, where the direction of the orthodontic load was varied from distal to mesial on the vestibular plane, with an increment of 6° in each experiment. To solidify our conclusion, we followed the Bland–Altman method [48] to validate the results. The Bland–Altman method is typically used to assess the agreement between two measurements that measure the same quantity. It involves plotting the differences between the two measurements against the average of the two measurements. Next, the mean difference and the limits of agreement are calculated. The mean difference indicates the systematic bias between the two measurements, while the limits of agreement provide information about the magnitude of the random error.

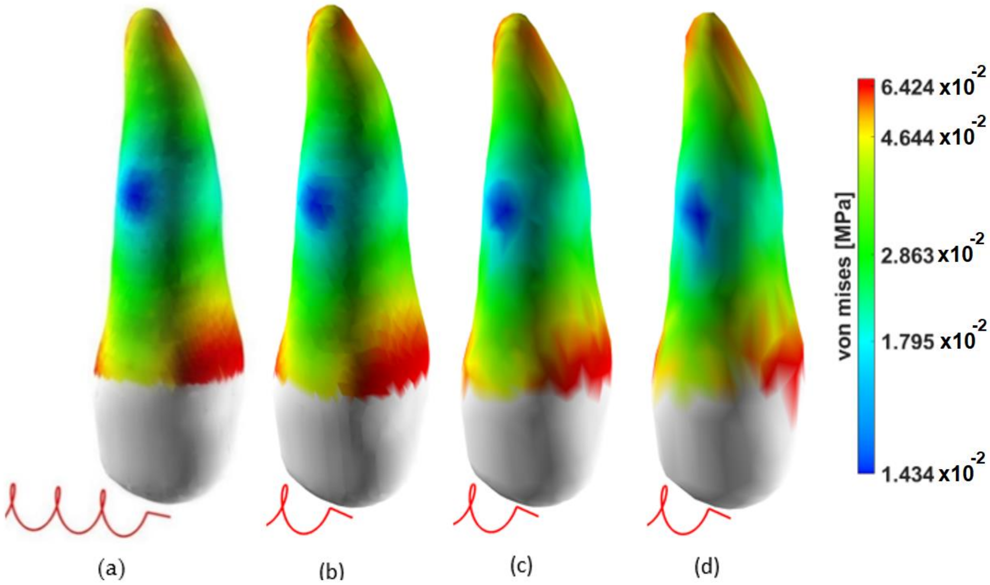

Figure 4. Upper right canine facet number optimization as OTM initiated before the remodeling process was ongoing. The red spiral represents the external force. (**a**) 26,608 facets, (**b**) 6652 facets, (**c**) 1662 facets and (**d**) 830 facets.

To implement this, a 100-bin histogram of the stress levels in each face resolution was generated. The area of each face was then normalized, such that the total area of the PDL faces was 1 in order to form an area distribution. Next, the histograms of the different resolutions were compared to that of the 26,608-facet resolution case (the maximal one). We also conducted a similar scenario with a 0.5 mm movement of the load anchorage on the tooth, where the remodeling process was ongoing (Figure 6). This experiment was also repeated 32 times for loads with the same orientations as described above.

The same process was repeated for a mandibular molar tooth that also includes a concave surface (Figure 7). A load of 300 gf (2.94 N) was positioned at the mid-buccal surface of models having 29,103 facets, 6834 facets, 1708 facets and 854 facets. The model was simulated during the instantaneous movement, until the remodeling process takes place (Figure 5).

The experiments of the canine and the molar tooth were repeated for a 0.5 mm anchorage movement, where the remodeling process was ongoing (see Figures 6 and 7). This experiment was also repeated 32 times.

One can conclude that 6652 facets suffices for the estimated requirement of 0.86% (1.4 KPa) accuracy compared with the maximal stress values in the 26,608-facet resolution for the canine case. For the molar case, 6834 facets suffice for a 2.1% (0.7 KPa) accuracy compared to the 29,103-facet resolution in the molar case.

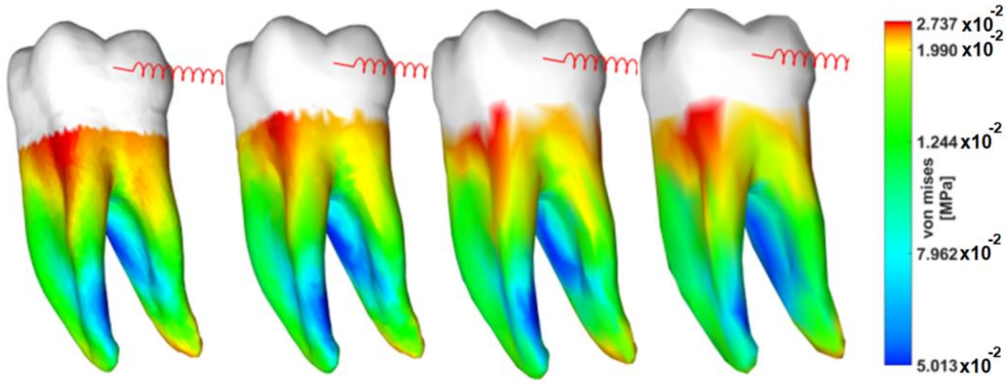

Figure 5. Facet number optimization as OTM initiated (before remodeling started) over a molar tooth. The red spiral represents the external force.

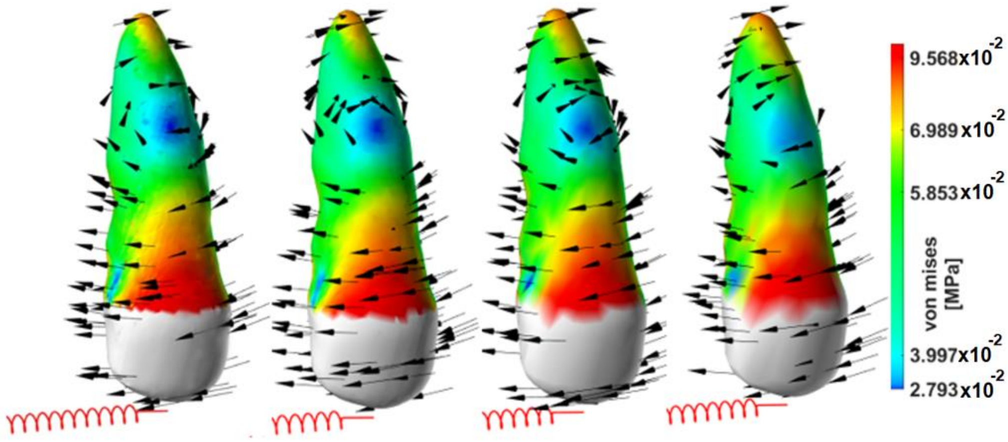

Figure 6. Comparison of stress on an upper right canine due to 2.94 N load after 0.5 mm anchorage movement. Black arrows plotted using [49]. The red spiral represents the external force.

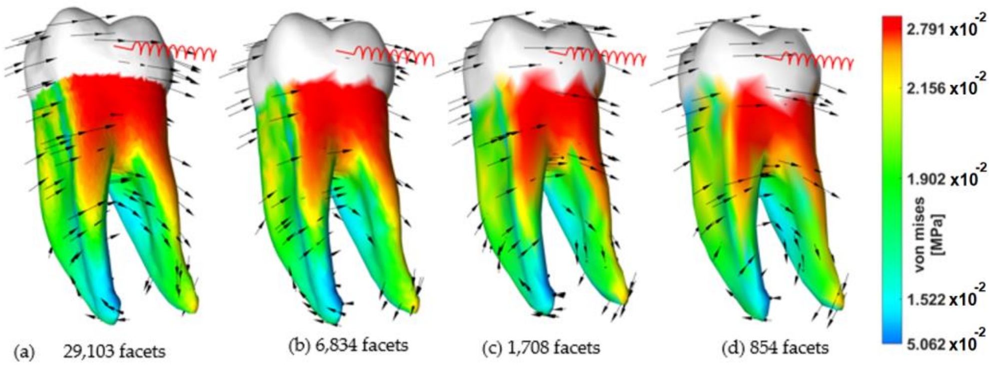

Figure 7. Comparison of stresses and movement for various facet resolutions in mandibular right molar after anchorage movement of 0.5 mm. Black arrows plotted using [49]. The red spiral represents the external force.

Note that Figures 6 and 7 demonstrate significant differences between the stress levels in the molar and canine teeth under the same load; this is due to the difference in the surface area size of the teeth. Similarly, to compare pairs of resolutions, for example, (a) and (b) in Figure 7, a Bland–Altman analysis was applied. Typical diagrams are provided in Figure 8 for the cases of the 6652- and 6834-facet resolution for the canine and molar cases, respectively.

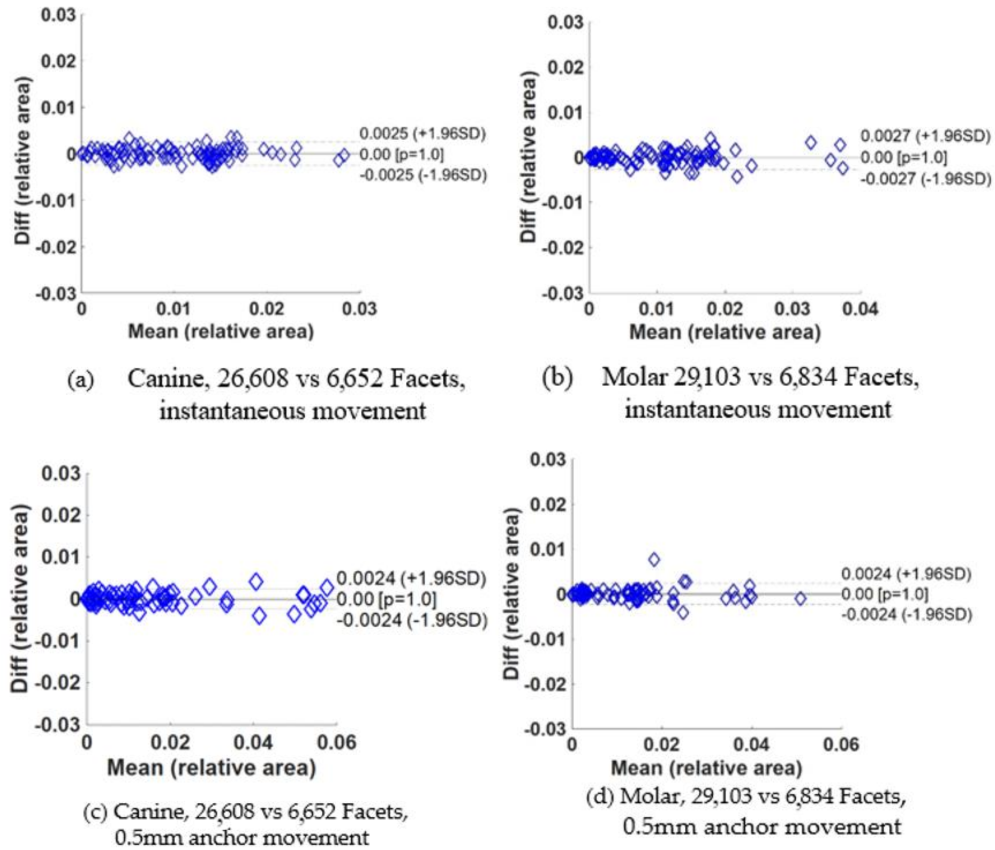

Figure 8. Bland–Altman plots of selected resolutions compared to the highest resolution. Values provided in units of SD.

The Bland–Altman plots for the low-resolution cases still demonstrated a significant agreement with regard to the highest one. As expected, lowering the number of facets increases the error standard deviation, as demonstrated in Table 4.

Table 4. The 95% confidence level (1.96) standard deviation of the produced Bland–Altman plots for lower resolutions. The benchmark resolutions are 26,608 facets for Canines and 29,103 for Molars.

Tooth & Resolution / Movement Type	Canine 1662 [SD]	Canine 830 [SD]	Molar 1708 [SD]	Molar 854 [SD]
Instantaneous movement	0.006	0.0096	0.0064	0.0104
0.5 mm movement	0.0055	0.0102	0.0064	0.0090

For conciseness, our study continues with the 6652-facet canine resolution in the following figures.

3.1. Validation

Intermediate Movement

The root surface of the simulated maxillary canine tooth is 2.64 cm^2, and the average root surface area is about 2.73 cm^2 [19,50]. The Modulus of Elasticity was taken as 0.68 MPa and the Shear Modulus G as 0.23 MPa. Applying these values implies that under a pulling force of $F = 2$ N located at the tooth center of rotation (i.e., a point where applying an orthodontic force will yield negligible rotation and mainly bodily movement), the mean normal stress is expected to be ∼7.4 kPa, which is indeed the case when remodeling is deactivated, and no tooth movement constraint is applied. Observe that some differences are expected when the angle of the PDL springs is subject to a predefined limitation (preventing them from entering the tooth body). The produced values were in close agreement with previous literature results published in [23].

To further validate the model, the results were compared to the study of Field et al. (2009) [12]. In their study, they applied the finite element method to analyze the mechanical responses due to orthodontic loading [12], which corresponds to our model when the remodeling process is suppressed. Thus, we ran the spring model introduced in this paper on the same scenario provided by Field et al. (2009) [12]. The results of our model and the reference model are provided in Figure 9; the results seem to match well. Further observe that as expected, both cases experience large strains in the alveolar crest and the apex.

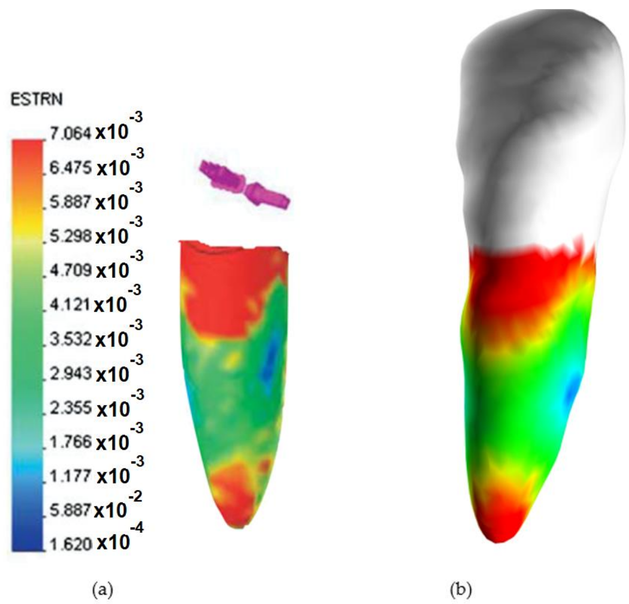

Figure 9. Comparison of equivalent strain [ESTRN] between a FEM study (**a**) by Field et al. [12] and (**b**) the proposed model. The colormap was adjusted to that used in [9] to allow convenient comparison and the same PDL properties as in [9], that is, ($E = 1.18$ Mpa, $\nu = 0.45$), the applied orthodontic force of 0.5 N (purple) was located at about the same location and angle as depicted in the reference. In both cases, the major strains are observed in the alveolar crest and the apex, as expected. Figure 9a provided courtesy of Prof. Michael Swain.

3.2. Remodeling Induced Movement

To validate the remodeling process, which is time-dependent and governed by a biological growth process, a limited real-time comparison was conducted; the model was implemented in MATLAB software on a 32 GB RAM Intel Core i7_9700 PC. A set of comparison tests on two healthy subjects with a total of four buccally erupted canines was used as clinical validation. The patients were 12 and 14 years old during a conventional orthodontic treatment with an orthodontic rubber band procedure. The subjects participated in this study after their legal guardians gave written informed consent, in accordance with the Ariel University ethical committee.

The layout of the teeth was imaged before and after a stage of orthodontic treatment (Figure 10). The applied initial force was 2.9 N, and the measured movement of the tooth anchorage was approximately 4 mm, with a rotation angle of 0.045 rad. The simulated movement of the tooth resulted in anchorage movement of 4 mm and a rotation angle of 0.0695 rad. The colors represent the von Mises stresses suggesting the highest values at the alveolar crest.

The brackets were attached to the canines, and a stretched orthodontic rubber (Chain plastic by American-Orthodontics, Sheboygan, WI, USA) was anchored to premolars; the measurements confirmed no premolar movement during treatment. The mechanical properties of the 0.6 mm thick orthodontic rubber were measured using a stress meter. Since the thickness of the bracket was 0.75 mm, the orthodontic appliance was assumed to be anchored $0.75 + 0.3 = 1.05$ mm away from the tooth. Our tests indicate a translational accuracy of <0.1 mm and rotational accuracy of <1°, which are below our measurement capabilities.

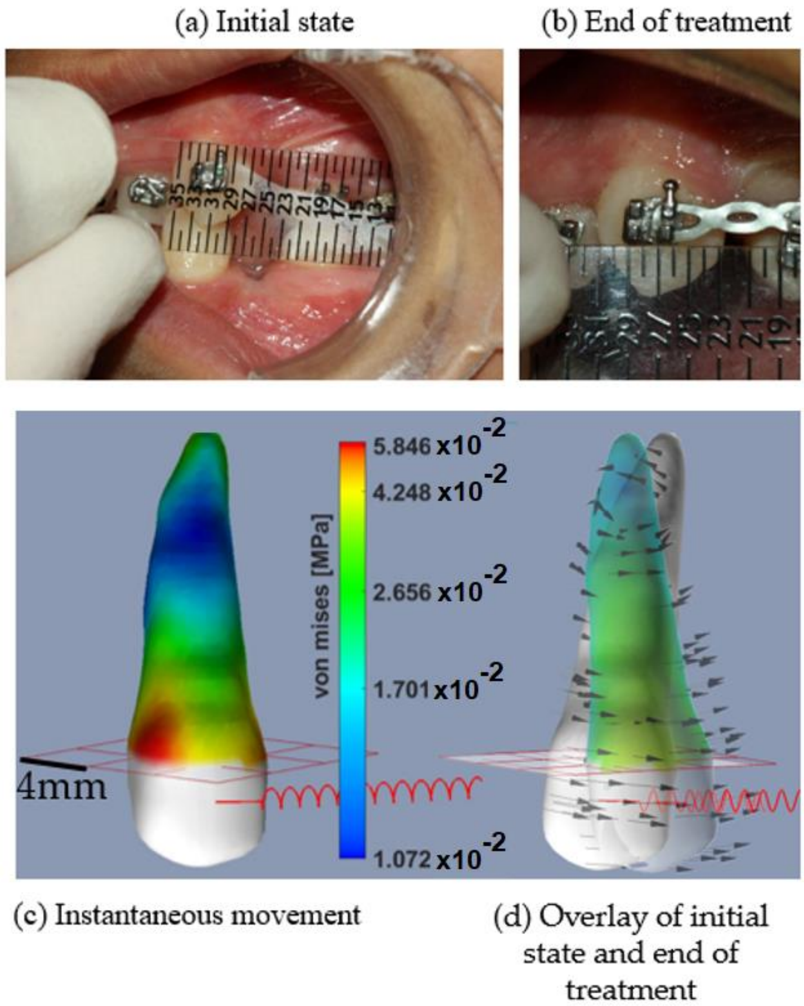

Figure 10. Comparison between a clinical case of orthodontic treatment conducted by one author and a model simulation (**a**,**b**). The clinical case before (**a**) and after treatment (**b**). The model at its initial configuration displaying the (von Mises) stresses before significant movement (**c**) and at the end of treatment, with an overlay of the original tooth position displayed in white (**d**). The gingival surface is displayed as a red mesh and the orthodontic appliance as a red coil. The applied initial force was 2.9 N, and the measured movement of the orthodontic tooth anchorage was approximately 4 mm. The anchorage is at the tooth power chain connection in (**a**,**b**) and at the edge of the red coil in (**c**,**d**). The tooth rotation angle was 0.045 rad.

For validating the model, it was compared to the clinical OTM cases of 4 canines in a pair of 12- and 14-year-old males, and the initial and final configurations were compared: the translation differences were negligible. In addition, the following differences in rotations were observed (rotation was measured around the camera view axis).

- Patient 1: Upper right canine—Clinical observed rotation: 6.88 [deg], Model observed rotation: 5.46 [deg], resulting in 1.42 [deg] of difference.
- Patient 1: Upper left canine—Clinical observed rotation: 2.61 [deg], Model observed rotation: 3.98 [deg], resulting in 1.37 [deg] of difference.
- Patient 2: Upper right canine—Clinical observed rotation: 4.01 [deg], Model observed rotation: 6.62 [deg], resulting in 2.21 [deg] of difference.

- Patient 2: Upper left canine—As the image taken did not allow accurate measuring of the rotation, we compared the orthodontic anchorage vertical Z-axis movement to measure our model's accuracy, which was measured at 0.1 [mm] in the clinical case, whereas in our numeric model, 0.31 [mm] was measured.

4. Discussion and Limitations

Throughout the paper, an isotropic PDL is assumed [18], and the orthodontic force was modeled as having a constant modulus of elasticity (cf. [51]).

Under these assumptions, it was noted that the von Mises stresses grow after the remodeling process is initiated. This is so as the tooth continues to move. Our results indicate that the remodeling process decreases the normal stress, allowing the tooth to further move; this can increase the shear stress faster than the relaxation rate. After a significant movement, the accumulated relaxation of the remodeling process compensates for the increased shear stress, resulting in the overall von Mises stress decrease. Figures 6 and 7 suggests that after a significant remodeling process occurs, the main contributors to the von Mises stresses' distribution are the shear stresses since the remodeling process relaxes the normal stress faster than it relaxes the shear stresses. This claim should be further examined; as the PDL is not an isotropic material, this may also imply updating Equation (6).

The importance of this study lies beyond that of engineering: as the algorithm provided here is rather fast (for example, calculating Figure 9 took five minutes on a MATLAB platform), one can create a "motion planning" algorithm to optimize the treatment time/forces applied, etc. [52]. In this regard, although there are studies in the field of biology, it is unknown to science what exactly governs the time duration of the remodeling process (this may depend, for example, on the exerted stress, the extent of the movement and the biological state of the tissue). Therefore, the time duration of each remodeling iteration in our scheme is obviously unknown. Nevertheless, having the model in hand, one may calibrate the time axis of the model by a set of controlled clinical OTMs.

It is worth noting that the current model can be utilized to address similar cases involving other teeth that are anchored using miniscrew-guided mechanics, while taking into account various diameters [53] and lengths [54]. In the general case, the forces applied on a treated tooth by neighboring teeth should be incorporated; we shall consider this in future work. The effect of both surrounding tissues—other teeth and bone—could be modeled by the same method under different conditions, as both could be calculated by the stresses of the PDL springs introduced. Lastly, a set of clinical conclusions may be derived from our method, for example, that when a tooth is vertically loaded (extrusion), the resulting stresses are lower than in the case where horizontal forces of the same magnitude are applied. This will be the focus of our future work.

5. Conclusions

We introduced a twofold model that includes the tooth's intermediate movement and the movement due to the biological growth of the loaded tissues (the remodeling processes). Although many studies that concern the former process are available in the literature, as it is well known to the orthodontic community, the lion's share of orthodontic tooth movement lies in remodeling, thus, the importance of this study. A set of experiments was carried out to validate our model and showed that it follows previous studies regarding the intermediate movement. Furthermore, a real-time in vivo clinical comparison demonstrated sufficient agreement with our model (approximately 2 [deg] and 0.3 [mm] errors), which indicates that the remodeling process is captured well by our scheme. The spring model introduced here is specifically designed to capture PDL tissue behavior and, therefore, reduces the required computational resources compared to available models in the literature. To examine this, a set of simulations under different resolutions was performed, and using Bland–Altman analysis, demonstrated that relatively low resolutions may indeed suffice.

Author Contributions: Conceptualization, N.S., O.M., S.Y. and R.S.; methodology, N.S., O.M. and S.Y.; software, S.Y.; validation, N.S., O.M., S.Y. and R.S.; formal analysis, N.S., O.M. and S.Y.; investigation, S.Y.; writing—original draft preparation, N.S., O.M., S.Y. and R.S.; writing—review and editing, N.S., O.M., S.Y. and R.S.; visualization, S.Y.; supervision, N.S., O.M. and R.S. All authors have read and agreed to the published version of the manuscript.

Funding: This research received no external funding.

Institutional Review Board Statement: The study was conducted in accordance with the Declaration of Helsinki, and approved by the Institutional Review Board (or Ethics Committee) of Ariel University AU-ENG-NS-20211207.

Informed Consent Statement: Informed consent was obtained from all subjects involved in the study.

Data Availability Statement: The data presented in this study are available on request from the corresponding author.

Conflicts of Interest: The authors declare no conflict of interest.

References

1. Cattaneo, P.M.; Dalstra, M.; Melsen, B. The finite element method: A tool to study orthodontic tooth movement. *J. Dent. Res.* **2005**, *84*, 428–433. [CrossRef] [PubMed]
2. Abraha, H.M.; Iriarte-Diaz, J.; Ross, C.F.; Taylor, A.B.; Panagiotopoulou, O. The mechanical effect of the periodontal ligament on bone strain regimes in a validated finite element model of a macaque mandible. *Front. Bioeng. Biotechnol.* **2019**, *7*, 269. [CrossRef] [PubMed]
3. Hasegawa, M.; Adachi, T.; Takano-Yamamoto, T. Computer simulation of orthodontic tooth movement using CT image-based voxel finite element models with the level set method. *Comput. Methods Biomech. Biomed. Eng.* **2016**, *19*, 474–483. [CrossRef] [PubMed]
4. Fill, T.S.; Carey, J.P.; Toogood, R.W.; Major, P.W. Experimentally determined mechanical properties of, and models for, the periodontal ligament: Critical review of current literature. *J. Dent. Biomech.* **2011**, *2*, 312980. [CrossRef] [PubMed]
5. Ferlias, N.; Dalstra, M.; Cornelis, M.A.; Cattaneo, P.M. In Vitro Comparison of Different Invisalign® and 3Shape® Attachment Shapes to Control Premolar Rotation. *Front. Bioeng. Biotechnol.* **2022**, *10*, 1–10. [CrossRef] [PubMed]
6. Li, P.; Kong, D.; Tang, T.; Di Su, D.; Yang, P.; Wang, H.; Zhao, Z.; Liu, Y. Orthodontic treatment planning based on artificial neural networks. *Sci. Rep.* **2019**, *9*, 2037. [CrossRef] [PubMed]
7. Shroff, B. *Biology of Orthodontic Tooth Movement: Current Concepts and Applications in Orthodontic Practice*; Springer: Berlin/Heidelberg, Germany, 2016.
8. Roberts, W.E.; Viecilli, R.F.; Chang, C.; Katona, T.R.; Paydar, N.H. Biology of biomechanics: Finite element analysis of a statically determinate system to rotate the occlusal plane for correction of a skeletal Class III open-bite malocclusion. *Am. J. Orthod. Dentofac. Orthop.* **2015**, *148*, 943–955. [CrossRef] [PubMed]
9. Provatidis, C.G. A comparative FEM-study of tooth mobility using isotropic and anisotropic models of the periodontal ligament. *Med. Eng. Phys.* **2000**, *22*, 359–370. [CrossRef]
10. Gupta, M.; Madhok, K.; Kulshrestha, R.; Chain, S.; Kaur, H.; Yadav, A. Determination of stress distribution on periodontal ligament and alveolar bone by various tooth movements–A 3D FEM study. *J. Oral Biol. Craniofacial Res.* **2020**, *10*, 758–763. [CrossRef]
11. Likitmongkolsakul, U.; Smithmaitrie, P.; Samruajbenjakun, B.; Aksornmuang, J. Development and validation of 3D finite element models for prediction of orthodontic tooth movement. *Int. J. Dent.* **2018**, *2018*, 4927503. [CrossRef]
12. Field, C.; Ichim, I.; Swain, M.V.; Chan, E.; Darendeliler, M.A.; Li, W.; Li, Q. Mechanical responses to orthodontic loading: A 3-dimensional finite element multi-tooth model. *Am. J. Orthod. Dentofac. Orthop.* **2009**, *135*, 174–181. [CrossRef] [PubMed]
13. Van Schepdael, A.; Sloten, J.V.; Geris, L. A mechanobiological model of orthodontic tooth movement. *Biomech. Model. Mechanobiol.* **2013**, *12*, 249–265. [CrossRef]
14. Geramy, A. Initial stress produced in the periodontal membrane by orthodontic loads in the presence of varying loss of alveolar bone: A three-dimensional finite element analysis. *Eur. J. Orthod.* **2002**, *24*, 21–33. [CrossRef]
15. Hemanth, M.; Raghuveer, H.P.; Rani, M.S.; Hegde, C.; Kabbur, K.J.; Vedavathi, B.; Chaithra, D. An Analysis of the Stress Induced in the Periodontal Ligament during Extrusion and Rotation Movements: A Finite Element Method Linear Study Part I. *J. Contemp. Dent. Pract.* **2015**, *16*, 740–743. [PubMed]
16. Dorow, C.; Krstin, N.; Sander, F.-G. Determination of the mechanical properties of the periodontal ligament in a uniaxial tensional experiment. *J. Orofac. Orthop./Fortschr. Der Kieferorthopädie* **2003**, *64*, 100–107. [CrossRef]
17. Ferguson, D.J.; Wilcko, M.T. Tooth movement mechanobiology: Toward a unifying concept. In *Biology of Orthodontic Tooth Movement*; Springer: Berlin/Heidelberg, Germany, 2016; pp. 13–44.

18. Wu, J.; Liu, Y.; Wang, D.; Zhang, J.; Dong, X.; Jiang, X.; Xu, X. Investigation of effective intrusion and extrusion force for maxillary canine using finite element analysis. *Comput. Methods Biomech. Biomed. Eng.* **2019**, *22*, 1294–1302. [CrossRef]
19. Zeno, K.G.; Mustapha, S.; Ayoub, G.; Ghafari, J.G. Effect of force direction and tooth angulation during traction of palatally impacted canines: A finite element analysis. *Am. J. Orthod. Dentofac. Orthop.* **2020**, *157*, 377–384. [CrossRef] [PubMed]
20. Burstone, C.J. The biomechanics of tooth movement. *Vistas Orthod.* **1962**, 197–213. [CrossRef]
21. Ren, Y.; Maltha, J.C.; Kuijpers-Jagtman, A.M. Optimum force magnitude for orthodontic tooth movement: A systematic literature review. *Angle Orthod.* **2003**, *73*, 86–92.
22. Lee, B.W. Relationship between Tooth-Movement Rate and Estimated Pressure Applied. *J. Dent. Res.* **1965**, *44*, 1053. [CrossRef]
23. Lee, B.W. The force requirements for tooth movement Part III: The pressure hypothesis tested. *Aust. Orthod. J.* **1996**, *14*, 93–97.
24. Hsu, M.L.; Chung, T.F.; Kao, H.C. Clinical applications of angled abutments-a literature review. *Chin. Dent. J.* **2005**, *24*, 15.
25. Turner, C.H.; Warden, S.J.; Bellido, T.; Plotkin, L.I.; Kumar, N.; Jasiuk, I.; Danzig, J.; Robling, A.G. Mechanobiology of the skeleton. *Sci. Signal.* **2009**, *2*, pt3.
26. McCormack, S.W.; Witzel, U.; Watson, P.J.; Fagan, M.J.; Gröning, F. The biomechanical function of periodontal ligament fibres in orthodontic tooth movement. *PLoS ONE* **2014**, *9*, e102387. [CrossRef]
27. Phannurat, P.; Tharanon, W.; Sinthanayothin, C. Simulation of surface mesh deformation in orthodontics by mass-spring model. *ECTI Trans. Electr. Eng. Electron. Commun.* **2011**, *9*, 292–296.
28. Dot, G.; Licha, R.; Goussard, F.; Sansalone, V. A new protocol to accurately track long–term orthodontic tooth movement. *J. Biomech.* **2021**, *129*, 9. [CrossRef]
29. Limbert, G.; Middleton, J.; Laizans, J.; Dobelis, M.; Knets, I. A transversely isotropic hyperelastic constitutive model of the PDL. Analytical and computational aspects. *Comput. Methods Biomech. Biomed. Eng.* **2003**, *6*, 337–345. [CrossRef]
30. Bourauel, C.; Freudenreich, D.; Vollmer, D.; Kobe, D.; Drescher, D.; Jager, A. Simulation of Orthodontic Tooth Movements. *J. Orofac. Orthop.* **1998**, *60*, 136–151. [CrossRef] [PubMed]
31. Provatidis, C.G. A Bone-remodelling Scheme Based on Principal Strains Applied to a Tooth During Translation. *Comput. Methods Biomech. Biomed. Eng.* **2003**, *6*, 347–352. [CrossRef] [PubMed]
32. Lee, R.J.; Weissheimer, A.; Pham, J.; Go, L.; de Menezes, L.M.; Redmon, W.R.; Loos, J.F.; Sameshima, G.T.; Tong, H. Three-dimensional monitoring of root movement. *Am. J. Orthod. Dentofac. Orthop.* **2015**, *147*, 132–142. [CrossRef]
33. Bouton, A.; Simon, Y.; Goussard, F.; Teresi, L.; Sansalone, V. New finite element study protocol: Clinical simulation of orthodontic tooth movement. *Int. Orthod.* **2017**, *15*, 165–179. [CrossRef] [PubMed]
34. Li, Z.; Yu, M.; Jin, S.; Wang, Y.; Luo, R.; Huo, B.; Liu, D.; He, D.; Zhou, Y.; Liu, Y. Stress distribution and collagen remodeling of periodontal ligament during orthodontic tooth movement. *Front. Pharmacol.* **2019**, *10*, 1263. [CrossRef]
35. Luchian, I.; Martu, M.-A.; Tatarciuc, M.; Scutariu, M.M.; Ioanid, N.; Pasarin, L.; Kappenberg-Nitescu, D.C.; Sioustis, I.-A.; Solomon, S.M. Using fem to assess the effect of orthodontic forces on affected periodontium. *Appl. Sci.* **2021**, *11*, 7183. [CrossRef]
36. Wu, J.; Liu, Y.; Li, B.; Wang, D.; Dong, X.; Zhou, J. Effects of different alveolar bone finite element models on the biomechanical responses of periodontal ligament. *Sheng Wu Yi Xue Gong Cheng Xue Za Zhi = J. Biomed. Eng. = Shengwu Yixue Gongchengxue Zazhi* **2021**, *38*, 295–302.
37. Dance, D.R.; Christofides, S.; Maidment, A.D.A.; McLean, I.D.; Ng, K.H. *Diagnostic Radiology Physics: A Handbook for Teachers and Students*; American Association of Physicists in Medicine, Asia-Oceania Federation of Organizations for Medical Physics, European Federation of Organisations for Medical Physics: Utrecht, The Netherlands, 2014.
38. Pauwels, R.; Jacobs, R.; Singer, S.R.; Mupparapu, M. CBCT-based bone quality assessment: Are Hounsfield units applicable? *Dentomaxillofacial Radiol.* **2015**, *44*, 20140238. [CrossRef] [PubMed]
39. Rees, J.S.; Jacobsen, P.H. Elastic modulus of the periodontal ligament. *Biomaterials* **1997**, *18*, 995–999. [CrossRef] [PubMed]
40. Coolidge, E.D. The thickness of the human periodontal membrane. *J. Am. Dent. Assoc. Dent. Cosm.* **1937**, *24*, 1260–1270. [CrossRef]
41. Jee, W.S. Principles in bone physiology. *J. Musculoskelet Neuronal Interact* **2000**, *1*, 11–13. [PubMed]
42. Chen, J.; Li, W.; Swain, M.V.; Darendeliler, M.A.; Li, Q. A periodontal ligament driven remodeling algorithm for orthodontic tooth movement. *J. Biomech.* **2014**, *47*, 1689–1695. [CrossRef]
43. Tanaka, E.; Inubushi, T.; Koolstra, J.H.; van Eijden, T.M.G.J.; Sano, R.; Takahashi, K.; Kawai, N.; Rego, E.B.; Tanne, K. Comparison of dynamic shear properties of the porcine molar and incisor periodontal ligament. *Ann. Biomed. Eng.* **2006**, *34*, 1917–1923. [CrossRef]
44. Hibbeler, R. Mechanics Of Materials. In *Mechanics Of Materials*; Prentice Hall: Hoboken, NJ, USA, 2011.
45. Medina, O.; Shapiro, A.; Shvalb, N. Minimal actuation for a flat actuated flexible manifold. *IEEE Trans. Robot.* **2016**, *32*, 698–706. [CrossRef]
46. Shvalb, N.; Moshe, B.B.; Medina, O. A real-time motion planning algorithm for a hyper-redundant set of mechanisms. *Robot.* **2013**, *31*, 1327–1335. [CrossRef]
47. Jones, R.M. *Deformation Theory of Plasticity*; Bull Ridge Corporation: Blacksburg, VA, USA, 2009; p. 151.
48. Altman, D.G.; Bland, J.M. Measurement in Medicine: The Analysis of Method Comparison Studies. *J. R. Stat. Soc.* **1983**, *32*, 307–317. [CrossRef]
49. arrow3 MATLAB Central File Exchange. 2023. Available online: https://ww2.mathworks.cn/matlabcentral/fileexchange/14056-arrow3 (accessed on 15 February 2023).

50. Jepsen, A. Root surface measurement and a method for x-ray determination of root surface area. *Acta Odontol. Scand.* **1963**, *21*, 35–46. [CrossRef]
51. Hwang, C.-J.; Cha, J.-Y. Mechanical and biological comparison of latex and silicone rubber bands. *Am. J. Orthod. Dentofac. Orthop.* **2003**, *124*, 379–386. [CrossRef] [PubMed]
52. Li, Z.; Li, K.; Li, B. Research on path planning for tooth movement based on genetic algorithms. In Proceedings of the 2009 International Conference on Artificial Intelligence and Computational Intelligence, Shanghai, China, 7–8 November 2009; Volume 1, pp. 421–424.
53. Sfondrini, M.F.; Gandini, P.; Alcozer, R.; Vallittu, P.K.; Scribante, A. Failure load and stress analysis of orthodontic miniscrews with different transmucosal collar diameter. *J. Mech. Behav. Biomed. Mater.* **2018**, *87*, 132–137. [CrossRef] [PubMed]
54. Jin, J.; Kim, G.-T.; Kwon, J.-S.; Choi, S.-H. Effects of intrabony length and cortical bone density on the primary stability of orthodontic miniscrews. *Materials* **2020**, *13*, 5615. [CrossRef]